AIChE WILEY InterScience DISCOVER SOMETHING GREAT

ENVIRONMENTAL AND ENERGY ENGINEERING

The Effect of CaO Sintering on Cyclic CO_2 Capture in Energy Systems

P. Sun, J. R. Grace, and C. J. Lim
Dept. of Chemical and Biological Engineering, University of British Columbia, Vancouver, BC, Canada V6T 1Z3

E. J. Anthony
CANMET Centre, Natural Resources Canada, Ottawa, ON, Canada K1A 1M1

DOI 10.1002/aic.11251
Published online July 20, 2007 in Wiley InterScience (www.interscience.wiley.com).

The importance of calcium-based sorbents, especially natural limestones, for CO_2 removal necessitates an investigation into the sorbent decay mechanism. This study starts from pore size distributions for samples from tests under various calcination/carbonation cycling conditions. A sintering model is formulated to describe the cyclic behavior of sorbents during cyclic calcination and carbonation. It explains the similar reversibility shown by sorbents under different test conditions. A balance between shorter cumulative sintering time and higher calcination rates appears to be responsible for the similar degrees of sintering and sorbent reversibility. © 2007 American Institute of Chemical Engineers *AIChE J,* 53: 2432–2442, 2007
Keywords: cyclic CO_2 capture, limestone, pore size distribution, sintering, modeling

Introduction

Calcium-based sorbents have been receiving increasing attention as possible candidates to remove CO_2 in situ from reactors, such as steam reformers, gasifiers, and water-gas shift reactors, where they can also improve hydrogen yields.[1–5] Calcium-based sorbents can also provide CO_2 removal from fluidized bed combustors (FBC).[6–11] Sorbent reversibility, i.e. decline of sorbent capability over multiple cycles, is a key factor affecting process economics for calcium-based CO_2 sorbents.[12] Among calcium-based sorbents, limestones are most appealing because of their high calcium-content, widespread occurrence and low cost.

Previous work on cyclic CO_2 removal with natural limestones shows that the reversibility of limestones decays according to a similar trend for a wide variety of test conditions.[9,10,13–17] Sintering of CaO is believed to be the major cause of deactivation, as evidenced by the change of sorbent surface texture after multiple cycles.[10,13,16,17] The surface textures of cycled limestones usually show growing macropores, as well as shrinkage of smaller pores.[16,17] These trends are typical of an intermediate sintering stage, described by sintering theory,[18] in which vacancies (or voids) generated by temperature- and ion-sensitive lattice defects direct void sites from smaller to larger ones, whereas the mass flow is from larger to smaller pores.

The importance of sintering of calcined limestones or their hydroxides has been studied because of the importance of limestones in high-temperature SO_2 capture.[19–25] Ionic compounds, such as CaO mostly sinter because of a volume diffusion or lattice diffusion mechanism. Borgwardt[19] introduced extremely mildly calcined CaO to a high-temperature oven to study sintering kinetics, confirming that the controlling sintering mechanism is through lattice diffusion. CO_2 and H_2O have also been reported to enhance CaO sintering.[20,26,27]

Sintering theory has not been previously applied to explain cyclic CO_2 capture. The mechanism behind the similar sorbent performance under a variety of test conditions also needs to be clarified. The aim of this work is to formulate and relate the sintering mechanism to sorbent cyclic behavior and to provide better understanding of cyclic CO_2 capture.

Correspondence concerning this article should be addressed to C. J. Lim at cjlim@chml.ca.

Experimental Studies

A fixed-bed thermogravimetric reactor (TGR) was used for the cyclic CO_2 capture tests. For comparison, one cyclic CO_2 capture run was also performed on a SHIMADZU TA60 thermogravimetric analyzer (TGA). All reactors operated at atmospheric pressure.

Further details of the TGR are provided elsewhere.[28,29] Mass flow controllers were utilized to achieve desired inlet gas concentrations. A total gas flow of 1600 ml/min was maintained at the reactor inlet for both calcination and carbonation in the TGR tests. Calcination temperatures were varied from 720 to 900°C. All carbonation reactions were carried out at 850°C with 100% CO_2 for a variety of times in different cycles to allow the fast stage of carbonation to go to completion. The TGA test featured 38–45 μm particles with 300 ml/min 100% N_2 flow for calcination and 300 ml/min 100% CO_2 for carbonation. Physical limitations were explored by varying operating parameters, e.g. particle and sample size and gas flow rate, to make sure that surface reaction was the rate-controlling step during calcination. In all the TGR and TGA runs, a 100% CO_2 atmosphere was maintained during heating from room temperature to the desired calcination temperature to prevent nonisothermal calcination. When suitable temperatures were reached, calcination was initiated by switching to 100% N_2. As both heating and cooling rates of the TGR were fast compared with the calcination process itself, the time needed to change between calcination and carbonation operating temperatures is considered negligible. Each calcination stage continued until no further mass decrease was observed.

Previous studies have shown that different natural limestones decay very similarly.[10,15,17] This leads to an assumption that the sintering kinetics for natural limestones are similar, probably because of their similar lattice diffusion behavior. Therefore, in this study, only one sorbent was used as a representative natural sorbent for the experimental and modeling study. Strassburg limestone particles of size ranges 38–45 μm and 212–250 μm were used for the TGR and TGA tests. Because of different bulk densities, 1 g of 212–250 μm or 0.5 g of 38–45 μm fresh particles was used at the start of TGR tests. In the TGA test, 4 mg of 38–45 μm fresh particles were used.

After the TGR tests, the sorbents were collected and stored in a desiccator. Samples were transferred to a Micromeritics 9300 Poresizer for pore size distribution (PSD) measurement. The highest pressure achievable in this instrument is around 197 MPa, corresponding to a pore size of 5.8 nm according to the Washburn equation.[30]

A separate PSD result based on N_2 adsorption showed that a 212–335 μm Strassburg calcine after initial calcination had a peak pore volume of ~30 nm, with limited pore volume residing at pores <6 nm, which are beyond the range of the mercury intrusion measurement employed in this work. Under these conditions, the specific surface area obtained by mercury intrusion data should approximate the BET values.[30] As a check, for initial calcines at 850°C, the two repeated specific surface area measurements by mercury intrusion gave 33 and 31 m^2/g respectively, whereas the BET method gave 36 m^2/g. The differences are believed to be due to the pores outside the range of mercury porosimetry, which, while low in pore volume, still contribute to surface area. Since the measured specific surface area is neither the main modeling objective nor input data in the current study, the specific surface area provided by mercury porosimetry is adequate for our purposes.

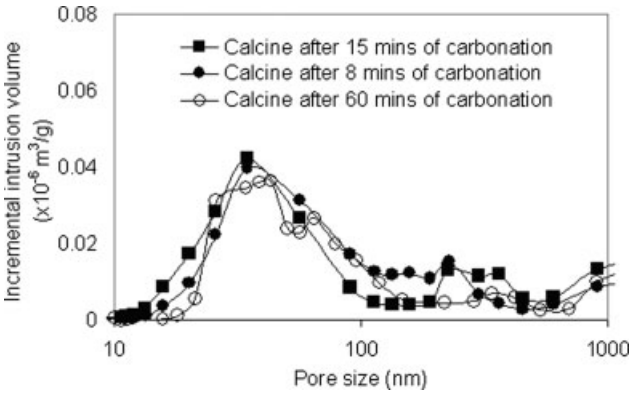

Figure 1. PSD: effect of carbonation time.

Experiments at 850°C for calcination and carbonation in TGR. 212–250 μm Strassburg particles. Calcination with 100% N_2; carbonation with 100% CO_2, fast stage completed.

Pore size distribution

The PSDs for calcines after different carbonation times in Figure 1 show that changing the carbonation time had negligible effect on the subsequent calcine structure. In these experiments, each carbonation step was allowed to proceed long enough to complete the fast stage. These results imply that lime sintering has no memory of carbonation history for the first cycle, or that carbonation makes no contribution to CaO sintering. It is believed that during calcination the recrystallization from $CaCO_3$ to CaO eliminates all structural differences caused by carbonation if without sintering. As discussed later, only extended carbonation (24 h or more) was capable of filling the intraparticle pores of highly cycled sorbents and hence able to rearrange the CaO to give a single-peaked pore structure. Since in this study, all the carbonation steps were only allowed to finish their fast portion, the calcination step is the sole stage considered for sintering.

To investigate whether the carbonation process experiences early pore blocking as is usually found for CaO sulphation, a calcined sample was carbonated long enough to allow the fast stage carbonation to be completed. The sample was split into two parts. One was then mildly ground into finer powder to expose blocked pores. Both carbonate samples were analyzed using mercury intrusion. Figure 2 compares the PSDs for the ground and the nonground carbonates, as well as their calcines, prior to being carbonated. No appreciable pore volume was found to be due to the blocked pores for runs under current test conditions. EDX mapping further indicated uniform carbon distributions over the particle cross-section as shown in Figure 3. (Note that the more concentrated carbon layer in the background was because of carbon-rich material used as sample bonders).

Figure 4 shows the PSDs for calcines with different calcination holding times at 850°C. Results show that without

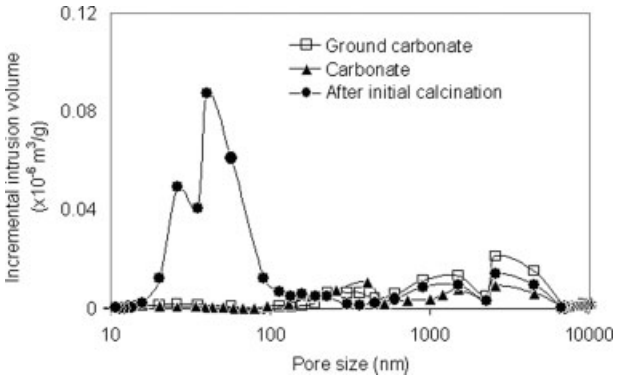

Figure 2. PSD for carbonate before and after mild grinding.

Same test conditions as in Figure 1.

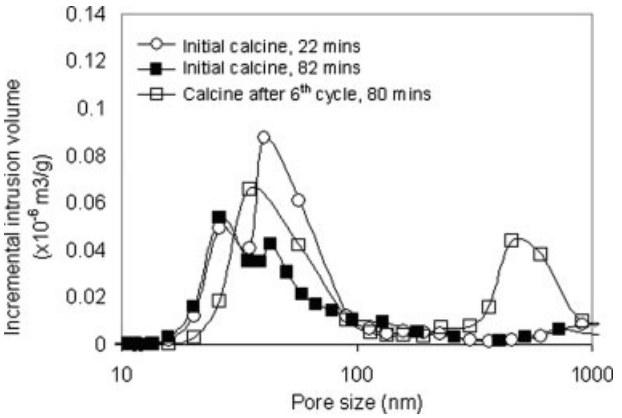

Figure 4. PSD: effect of calcination time or mode.

Same test conditions as in Figure 1.

cycling, longer holding times reduced the pore volume for pores <220 nm, but the pore distributions were all similar, with one major peak below <220 nm. Cycling the sorbent between carbonation and calcination for a cumulative holding time of 80 min resulted in a different PSD compared to the (single) run with initial calcination prolonged to 82 min. For the cyclic run, except for reduced volume of pores <220 nm (denoted V_1 pores), marked pore volume growth can be observed for pores larger than 220 nm (denoted V_2 pores). This indicates that sintering by holding calcines in N_2 is different from that after cyclic calcination/carbonation. The cycled samples with shrinkage of the smaller pores and simultaneous growth in the larger pores are typical of intermediate stage solid-state sintering.[18] Given that the presence of CO_2 is known to be able to accelerate sintering,[20,26,27] the cyclically released CO_2 during each calcination stage must be responsible for the development of the bimodal PSD.

The PSD results for calcines after different numbers of cycles in Figure 5 give further clear evidence of the development of bimodal distributions. Generally, with an increase in the number of cycles, the V_1 pore volume decreased, whereas the V_2 volume increased. Similar observations were reported by Abanades et al.[10]

To identify the upper limit of pore sizes in Figure 5, a SEM picture of a highly cycled calcine in Figure 6 shows that no pores larger than 1 μm can be observed on the

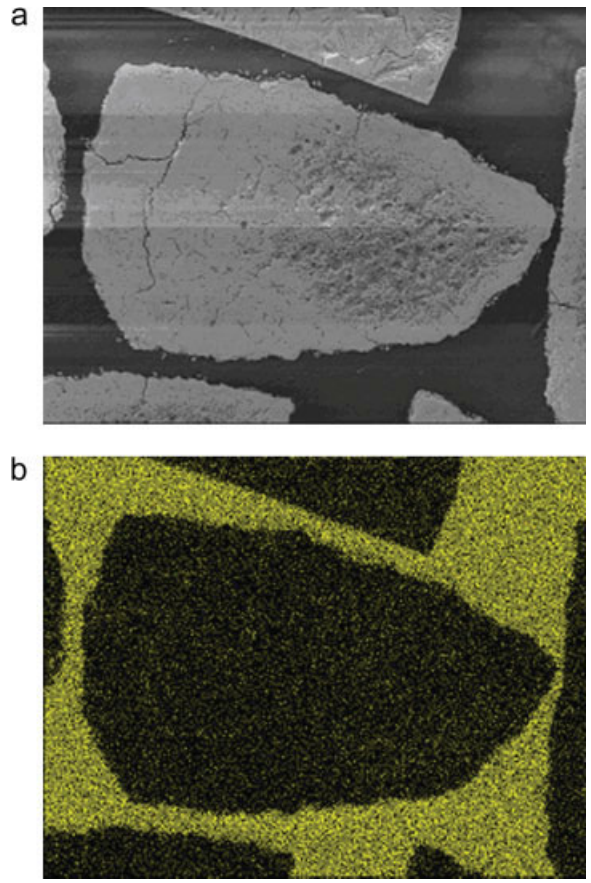

Figure 3. X-ray carbon mapping for carbonated Strassburg limestone (a) relative position of particles; (b) carbon distribution.

(Light white points represent carbon; background contains carbon-rich material). Same test conditions as in Figure 1. [Color figure can be viewed in the online issue, which is available at www.interscience.wiley.com.]

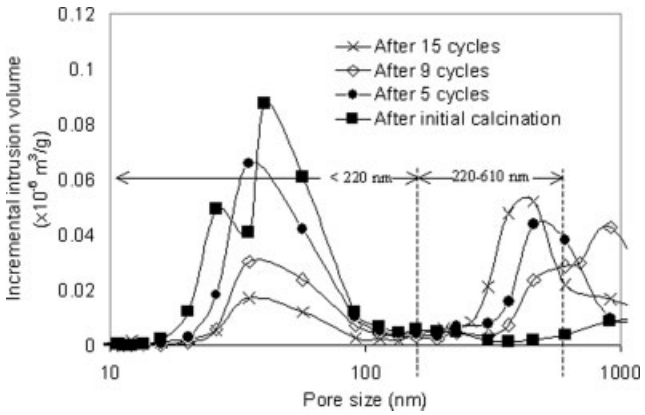

Figure 5. PSD: calcines after various number of calcination/carbonation cycles.

Test conditions as in Figure 1.

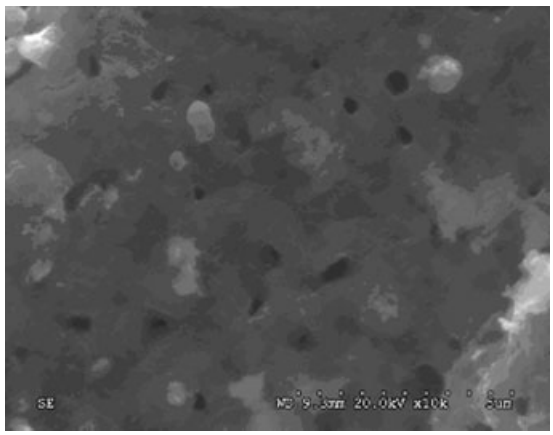

Figure 6. SEM pictures of cycled Strassburg calcine samples after 15 calcination/carbonation cycles at 850°C.

Test conditions as in Figure 1.

surface of the cycled sample. Thus the inflection point (at ~610 nm) in the range of 500–1000 nm in Figure 5 should mark the limiting size for the largest intraparticle pores. Pores larger than 610 nm are believed to be interparticle voids. Figure 5 also shows that there are clear divisions between the two pore size ranges, i.e. pores <220 nm and larger ones of 220–610 nm. 220 nanometer functions as a division line in this study, but it can also be applied to the work of Alvarez and Abanades[31] and Fennell et al.[32] The smaller pores presumably arise because of CO_2 being driving off during calcination, whereas the larger ones are due to sintering shifting vacancies from smaller to larger pores, driven by vacancy gradients.[18]

Model development

Pore Evolution During Cyclic Calcination/Carbonation. On the basis of the earlier observations, a model for pore evolution during cyclic operation is constructed. The pore evolution during cycling is believed to be responsible for the apparent decrease in CaO utilization. In the carbonation steps, a much slower reaction occurs when pores smaller than a critical pore diameter (~220 nm in this work) are filled. This phenomenon has been reported elsewhere.[13,15,16,33] To help clarify this for cyclic operation, the relationship between CaO utilization and available CaO porosity (defined as pore volume per unit particle volume) for carbonation is plotted in Figure 7, where the conversion of CaO to carbonate is based on porosity and given by,

$$X = \frac{\varepsilon_0}{(1/Z - 1)(1 - \varepsilon_0)} \tag{1}$$

The porosity is directly related to the measured specific pore volume V (m^3/g) by,

$$\varepsilon_0 = \frac{V}{V + \frac{1}{\rho_{CaO}}} \tag{2}$$

Hence porosity can refer to different assemblies of pores when different specific pore volumes are considered. In Figure 7, porosity based on both the total pore volume and pore volume below 220 nm were used in calculating CaO conversion. When the predictions are compared to the experimental CaO utilization in the TGR, good agreement is found for the V_1 pores, despite the scatter in overall pore volume measurement data. This further supports the contention that, on recarbonation, solid product $CaCO_3$ fills pores of small diameters (<220 nm). Once these pores are filled, the carbonation reaction becomes product-layer-controlled and proceeds at a much slower rate, with the carbonation product then slowly filling the V_2 pores. In other words, the pore volume of smaller-diameter pores (<220 nm) determines the achievable extent of carbonation during the fast stage of carbonation.

The specific surface area of calcines also decreases with increasing number of calcination/carbonation cycles. The specific surface areas after different numbers of cycles are shown in Figure 8 for experiments in which both the carbonation and calcination were carried out at 850°C with 212–250 μm Strassburg limestone particles.

Given that carbonation depends strongly on the smaller pores (V_1) and the monotonic decrease of pore volume of V_1 pores and specific surface area upon cycling, as well as the fact that pores of larger diameter contribute much less to surface area, the relationship between the pore volume of <220 nm pores and specific surface area is approximated by

$$dS = AdV_1 \tag{3}$$

with $S = S_g$ when $V_1 = V_g$; and $S = S_a$ when $V_1 = V_a$, where S_g and V_g are the initial specific surface area and specific pore volume. Subscript "g" refers to a "green state,"[18] an assumed state for freshly calcined limestones with zero degree of sintering, where the grains are ideally spherical. A value of $S_g = 70$ m^2/g is taken, the lower limit of the range (70–80 m^2/g) recommended by Mai and Edgar.[34] As different values are used in different models, sensitivity analysis

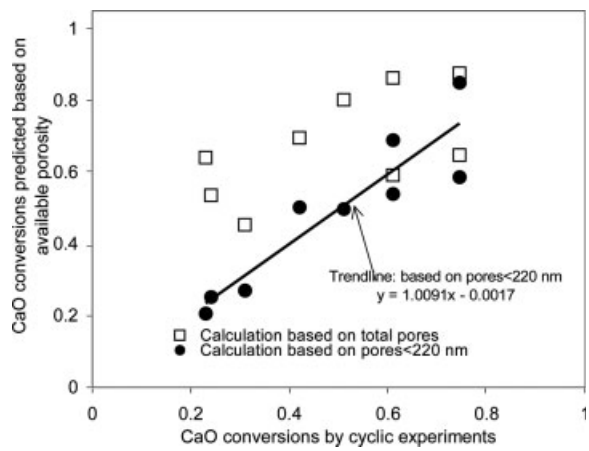

Figure 7. Conversion of CaO to $CaCO_3$: experiments vs. predictions with porosity (Eq. 1).

Experimental conditions: 850°C for calcination and carbonation in the TGR. 212–250 μm Strassburg particles. Calcination with 100% N_2; carbonation with 100% CO_2, fast stage completed.

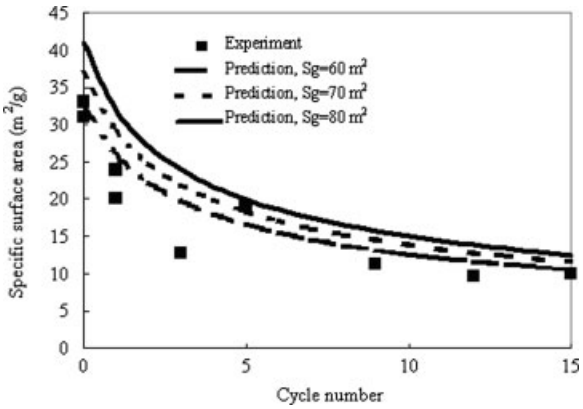

Figure 8. Specific surface area after each calcination cycle: experimental results versus predictions.

The predictions show the sensitivity to *S*g. Strassburg limestone in TGR, calcination at 850°C in 100% N_2; carbonation at 850°C in 100% CO_2. Fast stage of carbonation completed.

on this parameter is performed below. V_g is estimated from the theoretical maximum porosity ε_g:

$$V_g = \frac{\varepsilon_g}{\rho_{CaO}(1-\varepsilon_g)} \tag{4}$$

where ε_g is obtained from Eq. 1 with $X = 1$.

S_a and V_a are the asymptotic specific surface area and specific pore volume when the sample is sintered for an extremely long time. Various values, from 2 to 4 m^2/g, have been suggested for S_a.[21–25,34] A value of ~1.4 m^2/g is taken in this study as our separate BET data, using the five-point BET method for a CaO sample overnight-sintered at 1100°C, gave 1.4 m^2/g. Integration of Eq. 3 gives,

$$V_1 = \frac{(S - S_a)}{A} + V_a \quad A = \frac{(S_g - S_a)(1-\varepsilon_g)\rho_{CaO}}{\varepsilon_g} \tag{5}$$

On the basis of the earlier findings for cyclic calcination/carbonation, a pore evolution model is proposed as follows. It is assumed that after calcination with no sintering, CO_2 released during the calcination produces calcines with voids <220 nm and a single-peaked PSD in the green-state calcine. This is illustrated in Figure 9a, where V_1 pores are <220 nm within a unit volume occupied by the original nonporous limestone. However, in practice, calcination always involves sintering. During the initial calcination, the sintering, under the driving force of a surface energy gradient, directs ions to fill inter-granular space or vacancies to transfer from smaller to larger pore space. As sintering is occurring simultaneously with calcination, CO_2 mass flow could greatly enhance sintering of CaO along the path of the offgas flow. The net results of the process are shown in Figure 9b. The resulting pores consist of two parts: V_1 pores (<220 nm) related to the original calcination and V_2 pores (>220 nm) resulting from pore growth because of fast CO_2-catalyzed vacancy flow.

During subsequent carbonation, as portrayed in Figure 9c, reaction occurs in the smaller pores, and the CaO surface of the larger pores contributes little to the carbonation because of their low surface area. After the fast stage of carbonation is complete, all the V_1 pores (<220 nm) are filled, whereas V_2 pores are largely unfilled, serving as diffusion transport passages for further carbonation. During carbonation, CaO sintering is not considered, because the sintering-related mass flow of solid-state ions in V_1 is surpassed by the fast carbonation reaction, whereas for V_2, the surface energy is too small to permit appreciable sintering during carbonation.

The next sintering occurs during the next calcination stage. The sintering process is similar to the previous cycle, but with V_1 pores partially occupied during the last carbonation. As CO_2 is released and transported outward, the resulting pores, which should reproduce all of the V_1 pore volume if there were no sintering, could split into pores <220 nm (V_1) and those >220 nm (V_2) because of the sintering. The net results in Figure 9d, show further reduction in V_1 and growth in V_2 compared to the previous cycle portrayed in Figure 9b. The reduced pore volume in V_1 is used to accommodate carbonate during the next cycle. The pore volume in V_2 is additive during cycling. As V_1 continues to decrease, CaO utilization decreases accordingly. Note that the intermediate stage of sintering also involves a decrease in V_2 porosity, causing a decrease in total porosity.[18] But Eq. 5 eliminates the need to model total porosity change, and it is also found that the decrease in total particle porosity is modest (to ~0.46 for samples after 15 calcination/carbonation cycles at 850°C compared to 0.54 for the theoretical maximum porosity). It is believed that particle shrinkage only becomes dominant during the later state of the intermediate and final sintering stages. Therefore shrinkage of particles is neglected when considering calcination below.

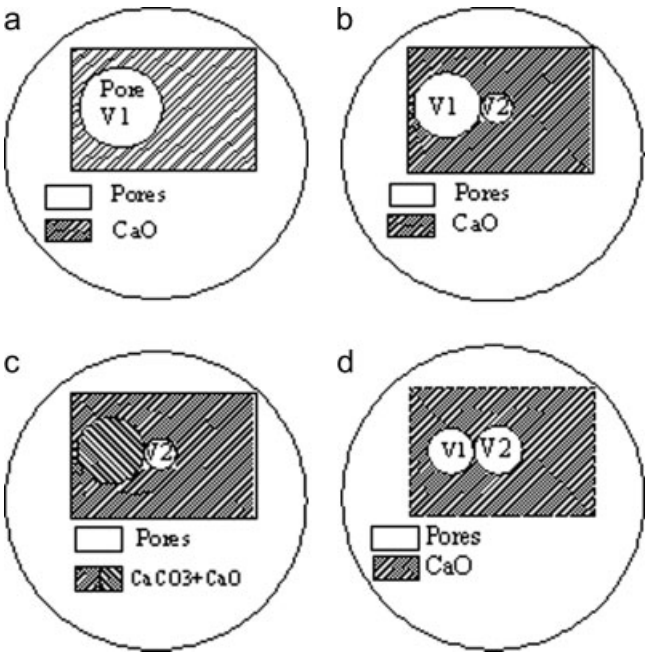

Figure 9. Schematic of sintering progression during cyclic calcination and carbonation.

(a) 1st calcination with no sintering; (b) After sintering, bimodal PSD; (c) After carbonation, smaller pores filled; (d) After re-calcination and sintering, pores further developer.

Reactor Model for Calcination. On the basis of the measurements discussed earlier, most CaO sintering occurs during calcination. To describe experimental cyclic calcination histories, a fixed bed was used for the TGR. The superficial velocity in the reactor was 0.1 m/s (850°C), but the actual in-bed gas velocity in the bed was lower because of gas bypassing, resulting in very low particle Reynolds numbers in the packed bed. For gas-solid flows at low Reynolds numbers (<1), the Peclet number (based on particle diameter) is small,[35] and axial dispersion has to be considered. Radial dispersion is not considered in this work. The control equation is written as,

$$u_{\text{bed}}\frac{\partial C(t,z)}{\partial z}-D_z\frac{\partial^2 C(t,z)}{\partial z^2}=\rho_{\text{CaCO}_3}(n)(1-\varepsilon_b)\frac{\partial X(t,z)}{\partial t} \quad (6)$$

The final term is related to the calcination rate for $CaCO_3$. In this equation, the time-derivative of $C(t,z)$ is omitted as it is usually negligible compared to other terms.[35] The bed voidage ε_b was chosen as 0.5 for the randomly packed bed of uniformly sized particles. u_{bed} is obtained by fitting the calcination time needed for the initial calcination. Once it is determined, it is assumed to apply also to the later cycles. In Eq. 6, time t is the calcination time. As discussed earlier, sintering accompanies calcination during each calcination/carbonation cycle. The time needed to complete each calcination stage is termed the calcination time for that cycle.

The boundary conditions are

$$\begin{aligned}&\text{At z} = 0, \quad C(t,z)=0\\ &\text{At z} = \text{L}, \quad \frac{\partial C(t,z)}{\partial z}=0\end{aligned} \quad (7)$$

In the reactor, the gas flowed downward from the top. At the top inlet, the CO_2 concentration is always zero. In Eq. 6, at a certain vertical position z, dX/dt describes the solid calcination rate to produce CaO at any bed location. Because limestone calcination is usually believed to proceed in a shrinking-core manner,[36,37] a shrinking core model (SCM) was used to express dX/dt. The SCM model was derived with the following rate law for calcination,

$$r = k_c[1 - C(t,z)/K_e] \quad (8)$$

where the equilibrium constant K_e is based on the correlation of Baker,[38]

$$K_e = 10^{(8308/T+7.079)}/(\text{R}_1\text{T}), \quad \text{mol/m}^3 \quad (9)$$

Kinetic data for limestone calcination suggested by Borgwardt[36] were adopted here:

$$k_c = 3.013 \times 10^7 \times \exp[-200/(\text{R}_1\text{T})], \quad \text{mol/m}^2\,\text{s} \quad (10)$$

The final expression for the SCM is then, at vertical position z,

$$\frac{dX}{dt}=\frac{1-\frac{C(z)}{K_e}}{\rho_{\text{CaCO}_3}(n)R\left\{\frac{1}{3k_mK_e}+\frac{(1-X)^{-2/3}}{k_c}+\frac{R}{3D_eK_e}[(1-X)^{-1/3}-1]\right\}} \quad (11)$$

where the mass transfer coefficient k_m ($=\text{Sh}D_o/R$), with the Sherwood number Sh calculated from the correlation suggested by Bird et al.[39] for creeping flow in packed beds.

$$Sh = 0.6(\text{Re}_p \times Sc)^{1/2} \quad (12)$$

The effective diffusivity, D_e, for CO_2 inside the porous lime layer is estimated from

$$D_e = D_0 \times \varepsilon_l^2 \quad (13)$$

The newly formed lime layer has a theoretical local porosity ε_l, assumed to be the theoretical maximum porosity ε_g. For calcined nonporous limestone, ε_g is around 0.54 based on a pore volume balance. As the current TGR calcinations have been found to be mainly controlled by gas-film mass transfer, the intraparticle mass transfer and surface reaction are not rate-limiting. Therefore, assuming this constant local porosity does not lead to appreciable errors, the correlation suggested by Levenspiel[40] for packed beds was adopted for the axial dispersion coefficient D_z.

The extent of decaying carbonation with cycling is reflected in the skeletal density of carbonate, i.e, if the CaO-$CaCO_3$ conversion achieved after the nth carbonation is $X_{\text{carb}}(n)$, during the (n + 1th) calcination, the density is taken as:

$$\rho_{\text{CaCO}_3}(n+1) = \rho_{\text{CaCO}_3,0}X_{\text{carb}}(n) \quad (14)$$

For the initial calcination of fresh limestone, $\rho_{\text{CaCO}_3}(1) = \rho_{\text{CaCO}_3,0}$.

Equation 6 was solved using a finite difference method. A downstream scheme was used for all differentiation terms, with the bed height divided into 20 equal intervals. Macroscopic variables, specific surface area, and CaO conversions were obtained by averaging over the cells as follows,

$$\bar{\Phi} = \frac{1}{L}\sum_{i=1}^{1=N}\Phi_i dl_{i_i} \quad (15)$$

Macroscopic Sintering During Cyclic Calcination/Carbonation Cycles. Sintering occurs simultaneously with calcination. On the macroscopic scale, the CaO surface area evolves as a result of both calcination and sintering. Hence

$$\frac{dS}{dt}=\left(\frac{dS}{dt}\right)_{\text{calcination}}-\left(\frac{dS}{dt}\right)_{\text{sintering}} \quad (16)$$

An empirical correlation was adopted to describe CaO surface evolution in the absence of sintering:

$$S = S_g X_{\text{carb}}(n)X \quad (17)$$

This gives $S = S_g X_{\text{carb}}(n)$ for complete calcination and 0 for 0 calcination. For the nth cycle,

$$\left(\frac{dS}{dt}\right)_{\text{calcination}} = S_g X_{\text{carb}}(n)\frac{dX}{dt} \quad (18)$$

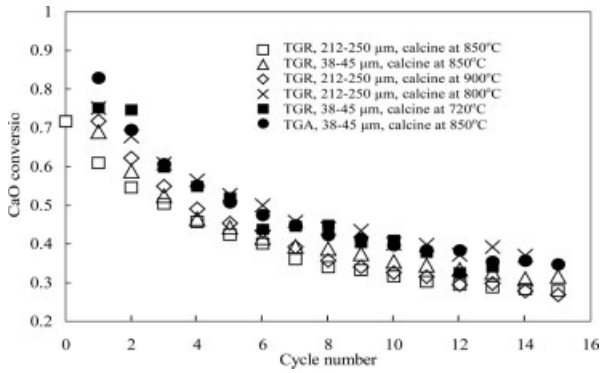

Figure 10. Reversibility under different test conditions in TGR or TGA, all with Strassburg limestone; calcination at 850°C in 100% N_2, carbonation at 850°C in 100% CO_2.

Fast stage of carbonation finished for each cycle of carbonation.

The CaO surface area reduction $\left(\frac{dS}{dt}\right)_{\text{sintering}}$ involves the sintering kinetics:

$$\left(\frac{dS}{dt}\right)_{\text{sintering}} = k_s(S - S_a)^2 \tag{19}$$

with

$$k_s = 2.45(1 + 10.3P_{CO_2}^{0.67})\ \exp(-29,000/T) \tag{20}$$

Equations 19 and 20, based on surface area reduction, have been adopted in studies on CaO sintering during calcination.[21–25,34] In Eq. 19 the quadratic dependence of sintering rate on surface area change was first proposed by Nicholson,[41] whereas in a similar sintering rate equation for intermediate-stage sintering, German[18] pointed out that the exponent should be related to the sintering mechanism. An obvious disadvantage of this equation is that when the reaction is under kinetic control, P_{CO_2} at the interface should closely approach the bulk CO_2 concentration, 0 in the current TGA test. Although in the TGA test calcination was completed more quickly, resulting in a shorter sintering time for each successive cycle, the cyclic performance showed similar decay behavior as in other TGR tests (Figure 10), indicating that sintering is still significant during the TGA test, probably due to accelerated calcination under TGA test conditions. Therefore, in this study, Eq. 20 is modified to include the calcination rate in the sintering rate expression,

$$k_s = 2.45\left\{1 + a\left[\frac{C_{CaCO_3,0}R}{k_c}\frac{dX}{dt}\right]^b\right\}\ \exp(-29,000/T) \tag{21}$$

where the activation energy of Eq. 20 is retained. Equations 21 and 19 were solved by a 4th order Runge-Kutta method with the initial condition that, at the start of calcination, the CaO surface area is zero.

At the end of the nth calcination, the $V_1(n)$ pore volume can be estimated by relating specific surface area as described by Eq. 5. $V_1(n)$ is then used to predict CaO conversions for the next carbonation based on a mass balance,

$$X_{\text{carb}}(n) = V_1(n) \times 56 \times \rho_{CaCO_3,0}/(1 - Z) \tag{22}$$

where 56 is the molecular weight of CaO, in g/mol.

Fitting Results

Figure 10 shows the reversibility under various test conditions. The general trends for different cyclic runs are seen to be very similar. As described earlier, these tests involve different particle sizes and sample sizes for both the TGR and TGA tests. Figure 10 indicates somewhat better reversibility at a lower temperature, e.g. 720°C, and for a small sample size, 4 mg for the TGA run, but the trend is not strong enough to draw clear conclusions. Results from the literature[9,16,17] indicate that different natural limestones give similar reversibility.

Table 1 summarizes the fitted results for u_{bed} based on the time needed for the initial calcination. The velocities in Table 1 are much smaller than the superficial velocity based on the cross-section area of the reactor (0.1 m/s). As a result, the particle Reynolds number is only about 0.04, and the Peclet number is only ~0.03 for a Schmidt number of ~0.7, justifying the inclusion of axial dispersion in the model.

Once u_{bed} is estimated in this manner, it is assumed to be unchanged for the following cycles. The fitted results for calcination history are shown in Figure 11 for three typical cycles where 212–250 μm Strassburg limestone was subjected to calcination/carbonation cycles at 850°C in the TGR. Although some deviation can be seen during the calcination history, the predictions of the current model generally fit the experimental data reasonably well. Values of a and b, determined by least square fitting using all experimental data from the six runs, are 1.26 and 0.59, respectively.

Discussion

Comparisons for all runs with these values of a and b are shown in Figures 12 and 13. The predictions are seen to agree reasonably well with the experimental data. The general decay trend of calcium utilizations is predicted by the current model. As described earlier, the degree of sintering is affected both by the duration of the calcination stage and by

Table 1. Fitted Results for u_{bed} (in Eq. 6)

Test No.	Test Conditions, °C/μm	u_{bed}, m/s
1	TGR, 850/212–250	0.012
2	TGR, 900/212–250	0.013
3	TGR, 800/212–250	0.011
4	TGR, 850/38–45	0.0105
5	TGR, 720/38–45	0.009
6	TGA, 850/38–45	Not needed

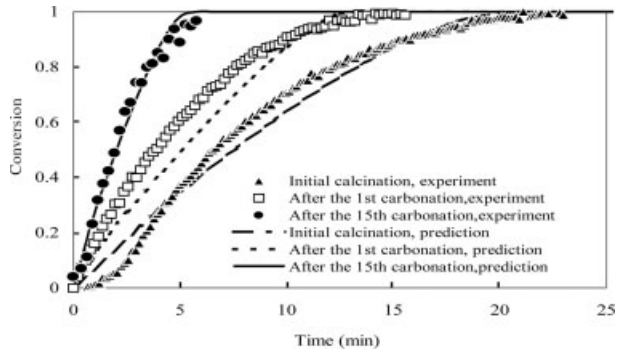

Figure 11. CaO conversion profiles for several calcination cycles: experimental results versus predictions.

212–250 μm Strassburg limestone in TGR; calcination at 850°C in 100% N_2, carbonation at 850°C in 100% CO_2. Fast stage of carbonation finished for each cycle of carbonation.

the sintering rate expressed by Eq. 21. These two effects could counterbalance each other to give similar sintering for different tests. For instance, the TGA test involved fast calcination or brief exposure under sintering conditions, but a much faster rate of CO_2 release, which should greatly accelerate the sintering rate, resulting in a similar sintering degree, as seen in Figure 13.

The fitted specific surface area for the run with 212–250 μm particles in the TGR is compared with measured data in Figure 8. The predicted specific surface areas are generally higher, but with a similar decay trend. Given that the specific surface area by mercury porosimetry is smaller than that obtained by the BET method, as discussed earlier, the model gives reasonable predictions. Predicted times for completion of the fast stage of calcination were in reasonably good agreement with experimental data as shown in Figure 14. When S_g was varied from 60 to 80 m^2/g, the model predictions were not sensitive to S_g as shown in Figure 14. However, Figure 14 also shows some obvious deviations for some tests, e.g. the model clearly underestimates calcination times for 850°C/212–250 μm and 720°C/38–45 μm runs. These deviations could arise from errors in determining experimental calcination time because of scatter in the experimental data as well as imperfection of the current model, such as the uncertain dependence on parameters like S_g, or the limitation of the current form of sintering rate law and kinetic data.

In a practical process for cyclic CO_2 capture, the sorbent would have to endure many more cycles than the number tested here. Despite losing capacity during cycling, if the highly sintered sorbent could maintain a residual CO_2 capture ability, it could be used affordably for a CO_2 removal process. Alvarez and Abanades[31] showed a ~10% residual CO_2 capture ability in a 100-calcination/carbonation-cycle study. In Figure 15, the model is extrapolated to 1000 cycles for three cases, TGR/850°C/231 μm, TGR/900°C/231 μm, TGA/850°C/41 μm, respectively. They generally give CaO conversion, 8.5–14% after 100 cycles, 4–6% after 500 cycles and 2.5–4.1% at 1000 cycles. Given the similarity for limestone reversibility, empirically regressed equations based on the extended prediction data are also shown in Figure 15, all with an exponential decay factor ~0.5. Considering that the current model overestimated the TGA/850°C/41 μm run and underestimated the TGR/850°C/231 μm run, the one based on the TGR/900°C/231 μm test,

$$X_{carb}(n) = 1.07(n+1)^{-0.49} \tag{23}$$

provides reasonable estimates for long-term limestone sorbent capture.

The current sintering model provides guidance on optimal CO_2 removal. As longer sintering time and higher calcination rate jointly control the degree of sintering, better CaO reversibility over long-time cycling may be achieved by adopting a lower degree of carbonation for each cycle. In this way the

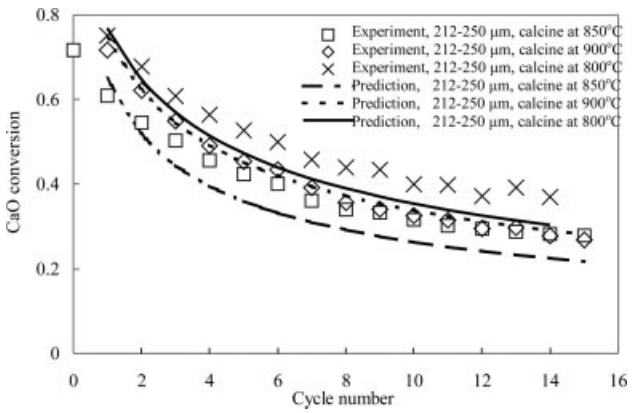

Figure 12. Reversibility: experimental results versus predictions for 212–250 μm Strassburg limestone in TGR.

Calcination at 850°C in 100% N_2; carbonation at 850°C in 100% CO_2. Fast stage of carbonations finished for each carbonation cycle.

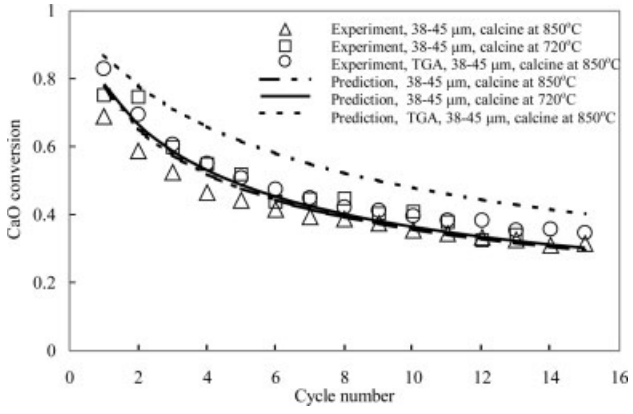

Figure 13. Reversibility: experimental results versus predictions for 38–45 μm Strassburg limestone in TGR or TGA.

Calcination at 850°C in 100% N_2, carbonation at 850°C in 100% CO_2. Fast stage of carbonations finished for each carbonation cycle.

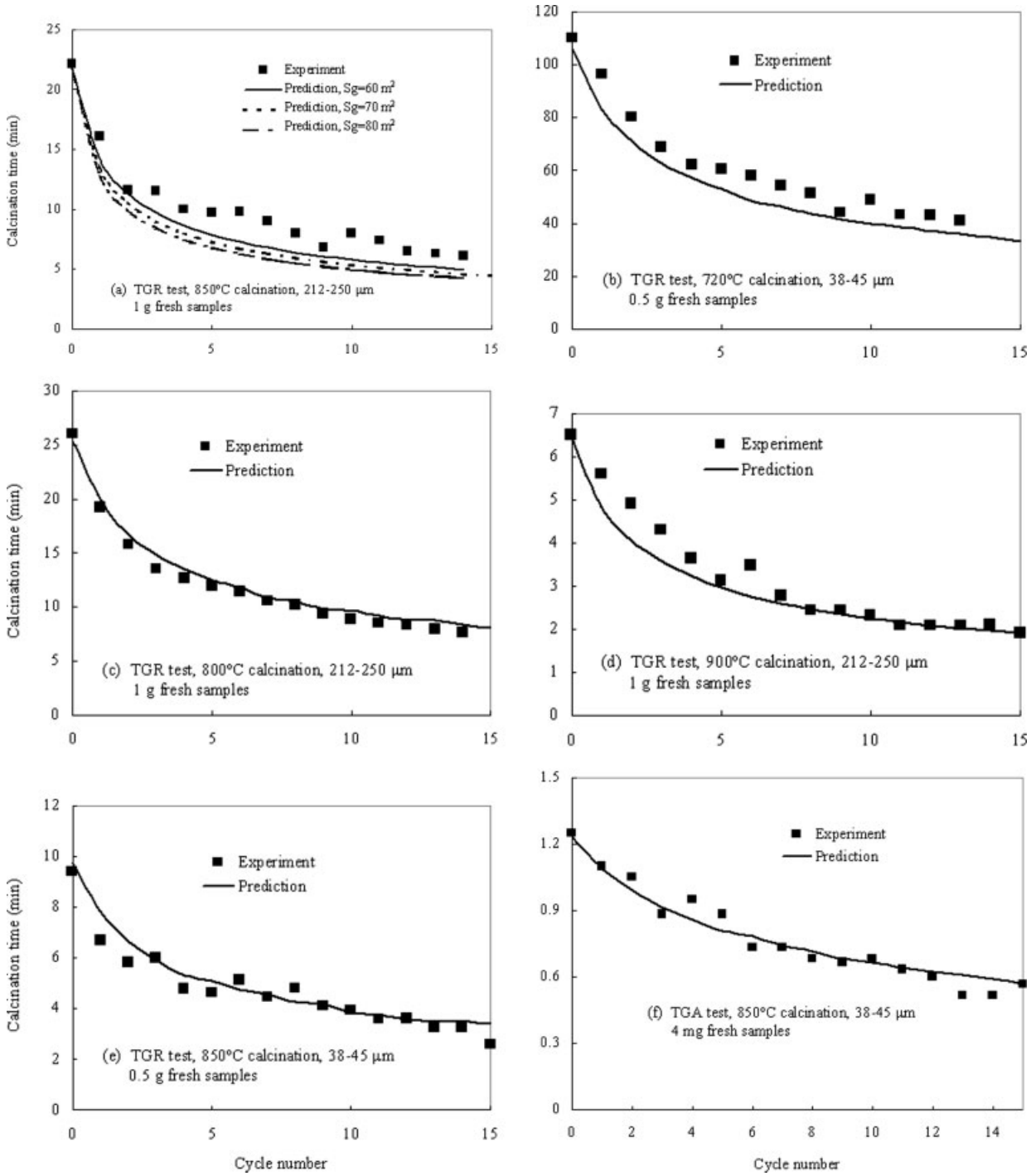

Figure 14. Calcination time: experimental results versus predictions.

Calcinations at 850°C in 100% N_2; carbonation at 850°C in 100% CO_2. Fast stage of carbonation finished for each carbonation step.

cumulative sintering time will be greatly shortened. Figure 16 shows experimental results for the effect of carbonation time on cyclic performance over 20 cycles. Under the given test conditions, 8 min was not enough to complete the fast stage of carbonation until after the 5th cycle. On the other hand, for the 3-min run where all carbonation periods lasted 3 min, the slower stage of carbonation was not reached over the entire 20 cycles, except for the 18th cycle that was deliberately extended to complete the fast carbonation stage. Given our finding that the extent of carbonation is determined by the pore volume of <220 nm pores, it is clear that for the same number of calcination/carbonation cycles, a shorter carbonation time retains more useful pore volume of <220 nm pores, likely because of the reduced cumulative

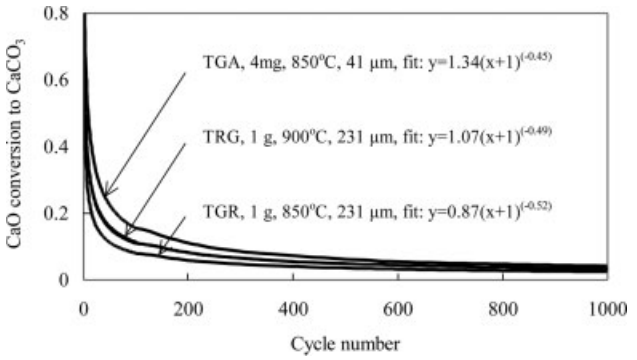

Figure 15. Predicted CaO utilization over 1000 cycles.

Same conditions for calculations as for Figures 12 and 13 in each case.

calcination time. (Recall that each calcination step was terminated when the weight stabilized). More experimental work is needed to investigate the performance beyond 20 cycles.

Another possibility would be to use a long carbonation time to reactivate highly cycled samples. This is because in most cyclic calcination/carbonation, V_1 pore volume monotonically decreases, whereas V_2 increases during cycling because V_2 pores are barely involved in the fast portion of carbonation. When the carbonation is allowed to proceed for such a long time that V_2 pores are gradually filled through slow product-layer-controlled carbonation, the subsequent calcination rearranges the PSD as if it were the initial calcination. Barker[13] demonstrated the effectiveness of one-day long carbonation on cycling, and this has recently been confirmed by Salvador et al.[9] However, the reactivated sorbents return to the normal decay trend when subjected to the cycling mode restricted to the fast early portion of carbonation.

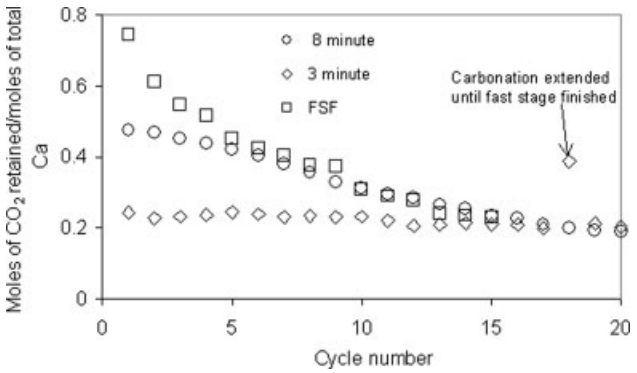

Figure 16. Effect of carbonation time on cyclic CO_2 capture performance: experimental results beginning with 850 mg of 212–250 μm fresh Strassburg limestone.

Calcinations at 850°C in 100% N_2; carbonation at 850°C in 100% CO_2. Carbonation time at each carbonation stage: FSF, Fast stage finished; comparing 3-min and 8-min cycles.

Conclusions

Investigation of samples obtained after different numbers of calcination/carbonation cycles showed that carbonation with the fast stage completed for each cycle had no influence on calcine pore size distribution. Cycling gives PSDs which differ greatly from those after one-time calcination, even if there is a similar cumulative time at the maximum temperature. All cycled samples showed bimodal PSDs, with a clear division between pores <220 nm and 220–610 nm pores. The volume of <220 nm pores decreased monotonically with continued cycling.

A sintering model based on experimental observations relates specific surface area to the volume of <220 nm pores. This portion of pores determines the calcium utilization achievable for the next fast stage of carbonation. A packed bed model and shrinking core model were used to predict cyclic calcination history, with a modified sintering kinetic model incorporated to describe specific surface area evolution. The predictions are in reasonable agreement with experimental data. There is little sensitivity to specific surface area, S_g. The model accounts for the similar reversibility of sorbents for the range of conditions tested. The balance between shorter cumulative sintering time and higher calcination rate can explain the similar degree of sintering. Extrapolation of the model suggests that the calcium utilization slowly decreases over cycling, eventually approaching zero, but this needs to be tested experimentally.

Notation

a, b = coefficients in Eq. 21
$C(t, z)$ = CO_2 concentration, mol/m^3
D_0 = CO_2 molecular diffusivity in N_2, m^2/s
D_e = effective diffusivity of calcined product layer
D_z = axial dispersion coefficient, m^2/s
i = cell number
k_c = calcination rate constant, mol/(s/m^2)
K_e = equilibrium CO_2 concentration, mol/m^3
k_m = mass transfer coefficient, m/s
k_s = rate constant for sintering, g/s/m^2
L = total bed height, m
l_i = ith bed cell height, m
N = total number of cells
R = particle radius, m
R_1 = gas constant, 8.314 $\times$ 10^{-3} in Eqs. 9 and 10, m^3 kPa/mol/K
Re_p = particle Reynolds number, = $2Ru_{bed}/v$
S = specific surface area for CaO, m^2/g
S_a = asymptotic specific surface area for CaO, taken as 1.5, m^2/g
Sc = Schmidt number, v/D_0
S_g = specific surface area for CaO with zero sintering, m^2/g
Sh = Sherwood number, defined in Eq. 12
t = calcination or sintering time, s
T = calcination temperature, K
u_{bed} = absolute gas velocity in the packed bed, m/s
V = total specific pore volume, m^3/g
V_1 = specific pore volume of pores <220 nm, m^3/g
$V_1(n)$ = specific pore volume of pores <220 nm after nth calcination, m^3/g
V_2 = specific pore volume of pores >220 nm, m^3/g
V_g = specific pore volume at green state, m^3/g
V_a = asymptotic pore volume, m^3/g
X = conversion of calcination when $CaCO_3$ is calcined, in Eq. 6
$X_{carb}(n)$ = CaO conversion after nth carbonation

z = distance from entrance of fixed bed, m
Z = molar volume ratio of calcine to carbonate for limestones, 0.46

Greek letters

Φ = macroscopic variables
ε_0 = porosity available for carbonation, m^3 pore/m^3 space
ε_b = bed voidage
ε_g = theoretical maximum porosity for complete calcination, 0.54
ε_l = theoretical local porosity of product layer
ν = kinematic viscosity of CO_2, m^2/s
ρ_{CaO} = skeletal density of CaO, 3.34×10^6, g/m^3
$\rho_{CaCO_3}(n)$ = molar density of $CaCO_3$ at start of nth calcination, mol/m^3
$\rho_{CaCO_3,0}$ = molar density of $CaCO_3$ in original limestone, mol/m^3

Literature Cited

1. Han C, Harrison DP. Simultaneous shift reaction and carbon dioxide separation for the direct production of hydrogen. *Chem Eng Sci*. 1994;49:5875–5883.
2. Ortiz AL, Harrison DP. Hydrogen production using sorption-enhanced reaction. *Ind Eng Chem Res*. 2001;40:5102–5109.
3. Lin SY, Suzuki Y, Hatano H, Harada M. Hydrogen production from hydrocarbon by integration of water-carbon reaction and carbon dioxide removal (HyPr-RING method). *Energy Fuels*. 2001;15:339–343.
4. Lin SY, Suzuki Y, Hatano H, Harada M. Developing an innovative method, HyPr-RING, to produce hydrogen from hydrocarbons. *Energy Convers Manage*. 2002;43:1283–1290.
5. Johnsen K, Ryu HJ, Grace JR, Lim CJ. Sorption-enhanced steam reforming of methane in a fluidized bed reactor with dolomite as CO_2-acceptor. *Chem Eng Sci*. 2006;61:1195–1202.
6. Shimizu T, Hirama T, Hosoda H, Kitano K, Inagaki M, Tejima K. A twin fluid-bed reactor for removal of CO_2 from combustion processes. *Trans IchemE*. 1999;77:62–68.
7. Gupta H, Fan F-S. Carbonation-calcination cycle using high reactivity calcium oxide for carbon dioxide separation from flue gas. *Ind Eng Chem Res*. 2002;41:4035–4042.
8. Abanades JC, Alvarez D, Anthony EJ, Lu D. In-situ capture of CO_2 in a fluidized bed combustor. In: *17th Inter Fluidized Bed Combustion Conference*, Jacksonville, Florida, USA, 2003; Paper 10:133–135.
9. Salvador C, Lu D, Anthony EJ, Abanades JC. Enhancement of CaO for CO_2 capture in an FBC environment. *Chem Eng J*. 2003;96:187–195.
10. Abanades JC, Anthony EJ, Alvarez D, Lu D, Salvador C. Capture of CO_2 from combustion gases in a fluidized bed of CaO. *AIChE J*. 2004;50:1614–1622.
11. Abanades JC, Anthony EJ, Wang J, Oakey JE. Fluidized bed combustion systems integrating CO_2 capture with CaO. *Environ Sci Technol*. 2005;39:2861–2866.
12. Abanades JC, Rubin ES, Anthony EJ. Sorbent cost and performance in CO_2 capture system. *Ind Eng Chem Res*. 2004;43:3462–3466.
13. Barker R. The reversibility of the reaction $CaCO_3 = CaO + CO_2$. *J Appl Chem Biotechnol*. 1973;23:733–742.
14. Silaban A, Harrison P. High temperature capture of carbon dioxide: characteristics of the reversible reaction between CaO(s) and CO_2 (g). *Chem Eng Commun*. 1995;137:177–190.
15. Abanades JC. The maximum capture efficiency of CO_2 using a calcination/carbonation cycle of $CaO/CaCO_3$. *Chem Eng J*. 2002; 90:303–306.
16. Abanades JC, Alvarez D. Conversion limits in the reaction of CO_2 with lime. *Energy Fuels*. 2003;17:308–315.
17. Sun P, Grace JR, Lim CJ, Anthony EJ. Removal of CO_2 by calcium-based sorbents in the presence of SO_2. *Energy Fuels*. 2006;21:163–170.
18. German RM. *Sintering Theory and Practice*. New York: Wiley, 1996.
19. Borgwardt RH. Sintering of nascent calcium oxide. *Chem Eng Sci*. 1989;44:53–60.
20. Borgwardt RH. Calcium oxide sintering in atmospheres containing water and carbon dioxide. *Ind Eng Chem Res*. 1989;28:493–500.
21. Silcox GD, Kramlich JC, Pershing DW. A mathematical model for the flash calcination of dispersed $CaCO_3$ and $Ca(OH)_2$ particles. *Ind Eng Chem Res*. 1989;28:155–160.
22. Mahuli SK, Agnihotri R, Jadhav RJ, Chauk S, Fan L-S. Combined calcination, sintering and sulfation model for $CaCO_3$-SO_2 reaction. *AIChE J*. 1999;45:367–382.
23. Milne CR, Silcox GD, Pershing DW, Kirchgessner DA. Calcination and sintering models for applications to high-temperature, short-time sulfation of calcium-based sorbents. *Ind Eng Chem Res*. 1990; 29:139–149.
24. Fuertes AB, Alvarez D, Rubiera F, Pis JJ, Marban G. Simultaneous calcination and sintering model for limestone particles decomposition. *Trans IchemE*. 1993;71:69–76.
25. Ghosh-dastidar A, Mahuli S, Agnihotri R, Fan L-S. Ultrafast calcination and sintering of $Ca(OH)_2$ power: experimental and modeling. *Chem Eng Sci*. 1995;50:2029–2040.
26. Ewing J, Beruto L, Searcy AW. The nature of CaO produced by calcite powder decomposition in vacuum and in CO_2. *J Am Ceram Soc*. 1979;62:580–584.
27. Beruto D, Barco L, Searcy AW. CO_2-catalyzed surface area and porosity changes in high-surface area CaO aggregates. *J Am Ceram Soc*. 1984;67:512–515.
28. Laursen K, Duo W, Grace JR, Lim CJ. Characterization of steam reactivation mechanisms in limestones and spent calcium sorbents. *Fuel*. 2001;80:1293–1306.
29. Laursen K, Duo W, Grace JR, Lim CJ. Sulfation and reactivation characteristics of nine limestones. *Fuel*. 2000;79:153–163.
30. Lowell S, Shields JE. *Powder Surface Area and Porosity*, 3rd edition. London: Chapman & Hall, 1991.
31. Alvarez D, Abanades JC. Pore-size and shape effects on the recarbonation performance of calcium oxide submitted to repeated calcination/recarbonation cycles. *Energy Fuels*. 2005;19:270–278.
32. Fennell PS, Pacciani R, Dennis JS, Davidson JF, Hayhurst AN. The effects of repeated cycles of calcination and carbonation on a variety of different limestones, as measured in a hot fluidized bed of sand. *Energy Fuels*; 2007; Article available on line: http://pubs3.acs.org/acs/journals/doilookup?in doi=10.1021/ef0605060o.
33. Bhatia SK, Perlmutter DD. Effect of the product layer on kinetics of the CO_2—lime reaction. *AIChE J*. 1983;29:79–86.
34. Mai MC, Edgar TF. Surface area evolution of calcium hydroxide during calcination and sintering. *AIChE J*. 1989;35:30–36.
35. Szekely J, Evans JW, Sohn HY. *Gas Solid Reactions*. London: Academic Press, 1976.
36. Borgwardt RH. Calcination kinetics and surface area of dispersed limestone particles. *AIChE J*. 1985;31:103–111.
37. Dennis JS, Hayhurst AN. The effect of CO_2 on the kinetics and extent of calcination of limestone and dolomite particles in fluidized beds. *Chem Eng Sci*. 1987;42:2361–2372.
38. Baker EH. The calcium oxide-carbon dioxide system in the pressure range 1–300 atmospheres. *J Chem Soc*. 1962;464–470.
39. Bird RB, Stewart WE, Lightfoot EN. *Transport Phenomena*, 2nd edition. New York: Wiley, 2002.
40. Levenspiel O. *Chemical Reaction Engineering*, 3rd edition. New York: Wiley, 1999.
41. Nicholson D. Variation of surface area during the decomposition of solids. *Trans Faraday Soc*. 1965;61:990–998.

Manuscript received Dec. 4, 2006, and revision received June 4, 2007.